RSC Advances

PAPER

View Article Online
View Journal | View Issue

Cite this: *RSC Adv.*, 2022, **12**, 20182

High electrochemical performance of ink solution based on manganese cobalt sulfide/reduced graphene oxide nano-composites for supercapacitor electrode materials†

Le Thi Thanh Tam, [a] Doan Thanh Tung, *[ab] Ha Minh Nguyet,[ab] Nguyen Thi Ngoc Linh,[c] Ngo Thanh Dung, [a] Nguyen Van Quynh,[d] Nguyen Van Dang,[c] Dimitra Vernardou,[e] Top Khac Le, [fg] Le Anh Tuan, [h] Phan Ngoc Minh*[b] and Le Trong Lu *[ab]

Received 4th May 2022
Accepted 6th July 2022

DOI: 10.1039/d2ra02818b

rsc.li/rsc-advances

Large scale supercapacitor electrodes were prepared by 3D-printing directly on a graphite paper substrate from ink solution containing manganese cobalt sulfide/reduced graphene oxide (MCS/rGO) nanocomposites. The MCS/rGO composite solution was synthesized through the dispersion of MCS NPs and rGO in dimethylformamide (DMF) solvent at room temperature. Their morphology and composition were investigated by scanning electron microscopy (SEM), transmission electron microscopy (TEM), and energy dispersive X-ray diffraction (EDS). The role of rGO on decreasing charge transfer resistance and enhancing ion exchange was discussed. The MCS/rGO electrode exhibits an excellent specific capacitance of 3812.5 F g^{-1} at 2 A g^{-1} and it maintains 1780.8 F g^{-1} at a high current density of 50 A g^{-1}. The cycling stability of the electrodes reveals capacitance retention of over 92% after 22 000 cycles at 50 A g^{-1}.

1. Introduction

Recently, electrochemical energy storage and conversion devices such as batteries, fuel cells, and supercapacitors have been widely studied for portable electronic devices, electric vehicles, storage and backup equipment, and emergency power systems.[1–3] Among various energy devices, supercapacitors (SCs) are of particular interest due to their superior properties such as super charging/discharging ability and high-power density.[4–6] Nevertheless, SC systems still exhibit drawbacks such as low specific energy density and high cost, leading to large size and difficult practical application.[7,8] Therefore, scientists often combine a pseudocapacitive mechanism with a double-layer capacitive mechanism to improve the quality of supercapacitors.[9–12]

Owing to their high electrical conductivity, large theoretical specific capacitance, and low cost, transition metal sulfides such as CoS, MnS, NiS, MoS, $CuCo_2S_4$ and $MnCo_2S_4$ have drawn growing attention as intriguing electrode materials for SCs.[5,13–16] Among them, binary metal sulfides have attracted more interest due to their multiple faradaic redox reactions.[3] Furthermore, these sulfide compounds present higher electrical conductivity than their monometal sulfide or oxide counterparts because the introduction of sulfur reduces the band-gap and facilitates electron transport.[17]

Chen *et al.* prepared three types of hollow tubular $M_xCo_{3-x}S_4$ structures (M = Mn, Ni, and Zn) for supercapacitor, where $MnCo_2S_4$ exhibits the best electrochemical performance with the specific capacitance of 1094 F g^{-1} at 10 A g^{-1}.[18] The fabrication of MCS material with various morphologies using hydrothermal, solvothermal, and electrochemical deposition has also been reported with specific capacitance up to 2400 F g^{-1}.[19–21] One can realize that it has not been studied much as a promising electrode for SCs, in spite of the fact that cobalt provides a larger oxidation potential and manganese delivers

[a]*Institute for Tropical Technology, Vietnam Academy of Science and Technology, 18 Hoang Quoc Viet, Hanoi 1000, Vietnam. E-mail: dtungtnt167@gmail.com; ltlu@itt.vast.vn*

[b]*Graduate University of Science and Technology, Vietnam Academy of Science and Technology, 18 Hoang Quoc Viet, Hanoi 1000, Vietnam. E-mail: pnminh@vast.vn*

[c]*Thai Nguyen University of Sciences, Tan Thinh Ward, Thai Nguyen City 25000, Thai Nguyen, Vietnam*

[d]*University of Science and Technology of Hanoi, Vietnam Academy of Science and Technology, Hanoi 1000, Vietnam*

[e]*Department of Electrical and Computer Engineering, School of Engineering, Hellenic Mediterranean University, 71410 Heraklion, Greece*

[f]*Faculty of Materials Science and Technology, University of Science, Ho Chi Minh City, 700000, Viet Nam*

[g]*Vietnam National University, Ho Chi Minh City, 700000, Viet Nam*

[h]*Phenikaa University, Nguyen Thanh Binh Street, Yen Nghia Ward, Ha Dong District, Hanoi, 12116, Vietnam*

† Electronic supplementary information (ESI) available. See https://doi.org/10.1039/d2ra02818b

more electrons favoring the rate capacity.[22] To date, the development of MCS electrode material is restricted because of their low rate performance at high current densities and short cycling stability.[23]

In order to overcome the limitations mentioned above about MCSs, one of the favorable approaches is the combination of MCS with nanocarbon-based material. Among carbon-based materials, reduced graphene oxide (rGO) has been widely applied as an efficient electrode material for SCs because of its great chemical stability, excellent electrical conductivity, and higher specific surface area.[3,24–26] As a consequence, the electrochemical performance of cathodes is expected to be improved due to the presence rGO.[27–31] In the MCS/rGO structure, MCS acts as a supporting agent to prevent the re-stacking of rGO sheets, while rGO acts as an interconnected porous matrix to support the anchoring of pseudo-charge ternary metal sulfides and provide excellent electron transport channels, resulting in improved capacitance, cycling stability, and rate capability. Currently, MCS/rGO nanocomposites can be fabricated by growing MCS materials directly on rGO surface or by the simple mixing of rGO with the as-prepared MCS materials.[28,29] However, in order to maximize the electrochemical performance of MCS materials, precisely controlled shape, size, composition and high phase purity are required. Therefore, it is better to prepare monodisperse MCS nanomaterials first and then assemble them onto rGO sheets, giving MCS/rGO composites with MCS size, shape, and composition well-defined.[30]

In our previous works,[32–35] high quality porous $CuCo_2S_4$–rGO electrode material for SCs was successfully fabricated by 3D printing technique. $CuCo_2S_4$ NPs were *in situ* grown on the surface of GO sheets under hydrothermal condition. The $CuCo_2S_4$–GO nanocomposite was then purified and redispersed in phenol to form printing ink solution. However, phenol is not good solvent for the dispersion of graphene materials due to their natural hydrophilic surface, which leads to irreversible agglomeration or restack of graphene sheets.[36,37] In addition, hydrothermal method requires autoclave leading to difficulties in scale-up. Thus, a judicious selection of a proper organic solvent with a strong interaction on the graphene sheets will possibly increase the dispersion and colloidal stability of the material in solution. In this work, dimethylform-amide (DMF) solvent was used to disperse materials in the form of rGO/MCS mixture at room temperature. Different electrode materials were fabricated by 3D-printer and their electrochemical characteristics were analyzed. The role of DMF solution of polyvinylpyrrolidone (PVP) to form MCS NPs/rGO sheets composites for SCs was clarified.

2. Experimental

2.1. Chemicals

The chemicals, manganese(II) chloride tetrahydrate 99%, cobalt(II) chloride hexahydrate 99%, 1-dodecanethiol 98% (DDT), 1-octadecene (ODE), dimethylform-amide 99% (DMF), graphite flakes, $KMnO_4$ 99.5%, H_2SO_4 98%, H_2O_2 30%, HCl, ascorbic acid 99%, polyvinylpyrrolidone (PVP), ethanol, and methanol were purchased from Sigma-Aldrich and directly used as received without any further purification. The graphite papers were supplied by Xiamen TOB new energy technology Co., Ltd, China.

2.2. Fabrication of MCS–rGO ink solution

The whole process for the preparation of MCS/rGO electrode is shown in Fig. 1. The GO sheets were prepared by modified Hummer's method.[31,32] Typically, 1.0 g of nature graphite flakes and 1.0 g of $KMnO_4$ were mixed in 35 mL of H_2SO_4 solution under overnight stirring. The reaction mixture was diluted in 300 mL of deionized water and 25 mL of H_2O_2. The solution was subsequently washed in 10% HCl under ultrasonic conditions. The GO solution was finally reduced by ascorbic acid to form rGO.

MCS NPs were synthesized by a thermal decomposition method with 1-dodecanethiol (DDT) acting as both sulfur source and surfactant.[32–34] Briefly, manganese(II) chloride tetrahydrate and cobalt(II) chloride hexahydrate with 1 : 2 molar ratio were added into three-neck, round bottom flask containing 1-octadecene (30 mL) and evacuated at room temperature for 30 min. The mixture was then heated to 140 °C, following with the quick injection of dodecanethiol (6 mL) as a sulfur source. The temperature of the reaction mixture was raised to 290 °C and kept constant for 60 min under continuous stirring. The solution was then cooled to room temperature. The MCS NPs were washed several times using a mixture of ethanol and methanol by centrifuging at 10 000 rpm for 5 min to obtain a black product. Finally, $NOBF_4$ was used as an exchange ligand to modify the surface of MCS NPs prior their dispersion into DMF solvent.

2.3. Fabrication of MCS–rGO electrode by 3D printing method

The ink solution based on MCS–rGO composites was fabricated by mixing 90 wt% active materials (including MCS NPs and rGO with the weight ratio of 1 : 1) and 10 wt% PVP as a binder in DMF solvent to form a printable solution.[30,38] The ink solution was coated on the graphite paper substrate of 2×1 cm^2 as the current collector by a modified 3D printer and kept for drying at around 100 °C to form MCS/rGO electrode.

2.4. Characterization

The morphology and elemental composition of the samples were analyzed using a transmission electron microscopy (TEM, JEM1010-JEOL), scanning electron microscopy (SEM, Hitachi S-4800) equipped with an energy-dispersive X-ray (EDX) spectroscopy. Crystalline structures of as-synthesized samples (rGO, MCS, and MCS/rGO) were characterized by X-ray diffraction analysis with Cu-Kα radiation and $\lambda = 1.5406$ Å. The surface areas of MCS material was determined by TriStar II 3020 device and calculated by the Brunauer–Emmett–Teller (BET) method.

The electrochemical properties of the electrodes were evaluated by cyclic voltammetry (CV), galvanostatic charge–discharge (GCD), and electrochemical impedance spectroscopy (EIS) techniques. The measurements were performed in a three-

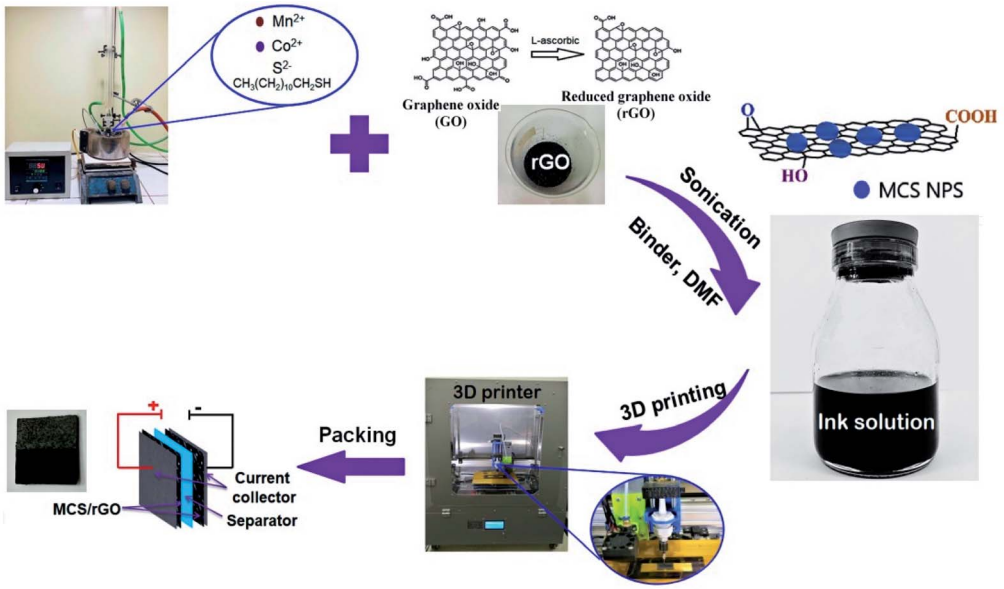

Fig. 1 Schematic illustration of the synthesis process for MCS/rGO electrode.

electrode configuration system using 6 M KOH solution as the electrolyte. The printed MCS–rGO nanocomposites electrode was used as the working electrode with the size of 2 × 1 cm^2, while the counter electrode was a platinum foil, and the reference electrode was a standard calomel electrode (SCE). The electrochemical potential window for all CV measurements at different scan rates was set in the range of −0.9 V to 0.1 V. EIS was also performed to study the synthesized material at a frequency ranging from 10 mHz to 100 kHz.

A symmetric full-cell supercapacitor assembled with two identical $MnCo_2S_4$–rGO electrodes, cellulose paper separator and 6 M KOH electrolyte, was tested in a two-electrode system.

3. Results and discussions

3.1. Morphology and phase structure

The TEM image of the MCS NPs (Fig. 2a) shows spherical nanoparticles with a mean size of 10 nm. The small size, high uniformity of MCS NPs with large specific surface area, will be easy to disperse uniformly when combined with rGO material in the ink solution facilitating more electrochemical active sites for faradaic redox reaction process.

The MCS/rGO ink solution in the DMF solvent is seen more intensely in Fig. 2b. Also, in Fig. 2c and d SEM images of rGO and MCS/rGO composites can be observed. It can be noticed that the rGO sheets are very thin with a wrinkled silk-like morphology and the MCS NPs are densely deposited on the surface of the rGO sheet after the mixing of MCS NPs and rGO sheets by ultrasonic vibration. The good dispersion of the MCS NPs on the surface of the rGO sheets prevents the re-stacking of the rGO sheets and forms a large amount of void space, creating an interlaced structures in the composite, which is conducive to excess electrolyte interaction and redox reactions at high current densities. This is in accordance with the aforementioned results for the electrochemical properties of the MCS/rGO electrode.

The combination of rGO and MCS nanoparticles aims to enhance the specific surface area of the supercapacitor electrode. Fig. S1† shows the results of the surface analysis with a high BET surface area value of 836 $m^2\ g^{-1}$. This demonstrates that the intercalation of MCS nanoparticles between the rGO sheets significantly increases the specific surface area and leads to a higher increase in the double-layer capacitance value.

Fig. 3a shows XRD patterns of the rGO, MCS, and MCS/rGO. The XRD spectrum of rGO samples consists of only one peak at $2\theta = 26.5°$ corresponding to graphene, indicating the effective reduction of GO to rGO.[34] Simultaneously, the XRD data of MCS NPs presents multi peaks around 30.9°, 38.2°, 49.9°, and 55.3°, which are indexed to (311), (400), (511), and (440) planes of Co_3S_4 (JCPDS no. 42-1448).[3] In addition, there are no diffraction peaks of manganese sulfide, demonstrating manganese element has partially replaced cobalt ions in the lattice structure. Therefore, the chemical formula of MCS could be speculated to $Mn_xCo_{3-x}S_4$ where $0 < x < 3$. XRD spectrum of MCS/rGO composites reveals the same peak positions with MSC sample, but with lower intensity due to the construction of rGO with MCS NPs.

Furthermore, the composition and purities of the MCS/rGO composites are confirmed by EDX. Fig. 3b reveals the composition of Co, Mn, S, C, and O. The atomic ratio of Co/Mn = 8.07/3.84 is very close to the Co/Mn ratio in $MnCo_2S_4$. In the thermal decomposition reaction, DDT not only acts as a source of sulfur, but also as a capping agent and surfactant. It is even used as a reducing agent in the synthesis of MCS NPs. ODE is employed as the reaction medium for the chloride salt precursors to allow the reactions to be carried out.

In order to investigate the distribution of components in the ink, the ink was printed on the graphite substrate and EDX

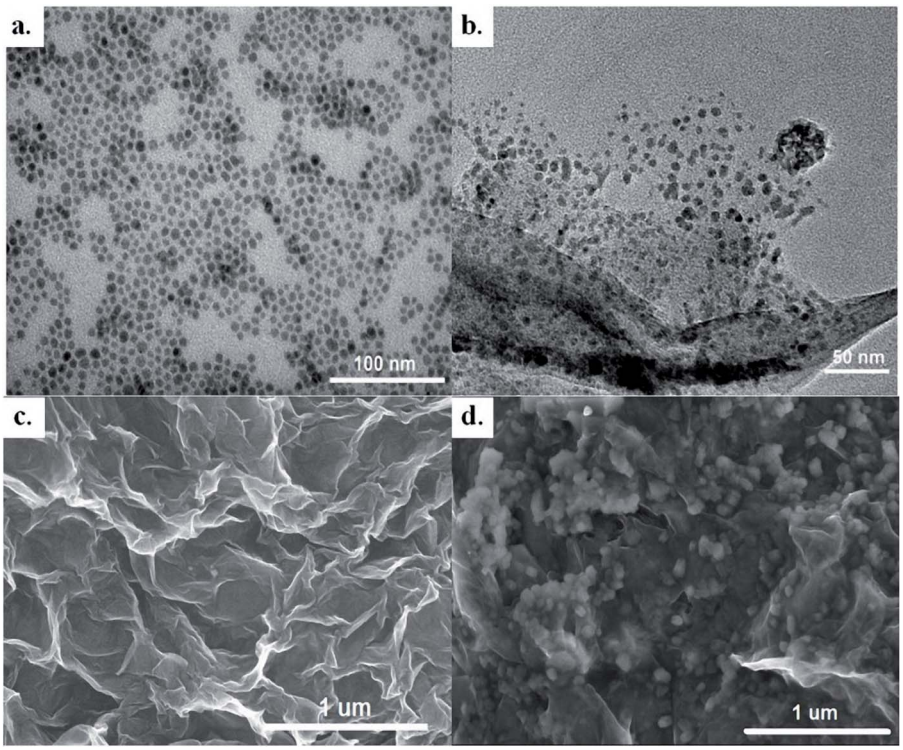

Fig. 2 TEM images of MCS NPs and MCS/rGO (a and b) and SEM images of rGO and MCS/rGO (c and d).

mapping was performed. In Fig. 3c, the elements (C, Mn, Co and S) are very uniformly dispersed over the entire electrode surface. This proves that the MCS nanoparticles and rGO are well dispersed in the DMF solvent.

3.2. Electrochemical properties

Fig. 4a compares the electrochemical characteristics of four electrodes, *i.e.* graphite substrate, rGO/graphite substrate

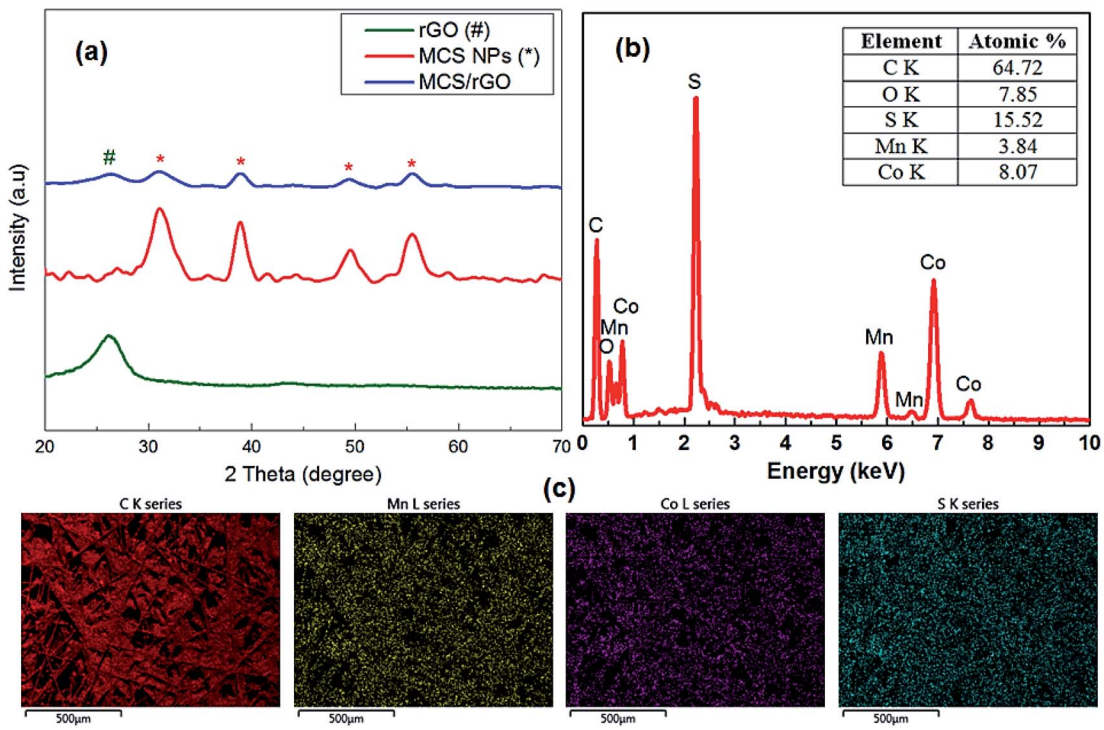

Fig. 3 (a) XRD patterns of rGO, MCS and MCS/rGO composite; (b) EDS spectrum of the MCS/rGO composite; (c) EDS mapping of the MCS/rGO composite.

(denoted as rGO), MCS/graphite substrate (denoted as MCS), and MCS/rGO/graphite substrate (denoted as MCS/rGO). The capacitance contribution of the graphite paper substrate is negligible and can be ignored. The rGO material contributes almost exclusively to the electric double-layer effect. The CV curve of rGO presents a quasi-rectangular shape and has no obvious redox peaks showing similar behavior with carbon-based materials.[39] Meanwhile, the MCS material shows the ability to contribute both electric double-layer and pseudo-capacitive effects. It has a rather high redox peak at a potential of about −0.05 V. The specific capacitances of MCS, rGO and MCS/rGO are 2097, 409, and 3338.5 F g^{-1} at the scan rate of 5 mV s^{-1}, respectively. It can be seen that the capacitance value increases significantly when combining MCS nanoparticles with rGO. This is possible due to the intercalation of rGO sheets with MCS nanoparticles increasing the contact area of the supercapacitor electrode with the electrolyte and increasing the charge transfer capacity. Therefore, the synergy of rGO and MCS is important to obtain superiority in performance. The CV curve of the MCS/rGO composite shows that the area of the CV curve has been increased and still retains the typical redox peaks of MCS. The redox peaks of MCS and MCS/rGO electrode originate from the interaction between S^{2-}, $Co^{2+}/Co^{3+}/Co^{4+}$ and Mn^{2+}/Mn^{3+} ions, which is described by the following reversible reactions:[40–46]

$$MS + OH^- \leftrightarrow MSOH + e^- (M = Co, Mn)$$

A lot of pseudo-capacitive materials for supercapacitors are usually quite sensitive to the effects of voltage and current changes during their operation because these are related to the speed and efficiency of the reversible reactions. The CV curves of MCS/rGO (Fig. 4b) at different scan rates from 5 to 50 mV s^{-1} in the potential window of −0.9–0.1 V (*vs.* SCE) present a similar quasi-rectangular shape with the distinct pairs of redox peaks, indicating that the capacitance is attributed to the combination of EDLC mechanism of rGO and pseudocapacitance mechanism of manganese cobalt sulfide material. The curves also reveal the increase of the current densities with increasing scan rates, proving excellent diffusion of ions at the interface between the electrode and the electrolyte. Furthermore, the positions of the oxidation and reduction peaks move to higher and lower potentials respectively when the scan rate increases, which is mainly attributed to the polarization effect of the electrodes.[5,47] Additionally, the shape of CV curves is maintained even at the high scan rate of 50 mV s^{-1}, indicating superior electron transport kinetics, and excellent rate performance of MCS/rGO electrode.

Fig. 4c illustrates the GCD plots of the as-synthesized MCS/rGO electrode at various current densities ranging from 2 to 50 A g^{-1}. According to the GCD curves, the specific capacitance (C_{sp}) can be acquired as shown below:[48]

$$C_{sp} = \frac{I\Delta t}{m\Delta V} (\mathrm{F\ g^{-1}})$$

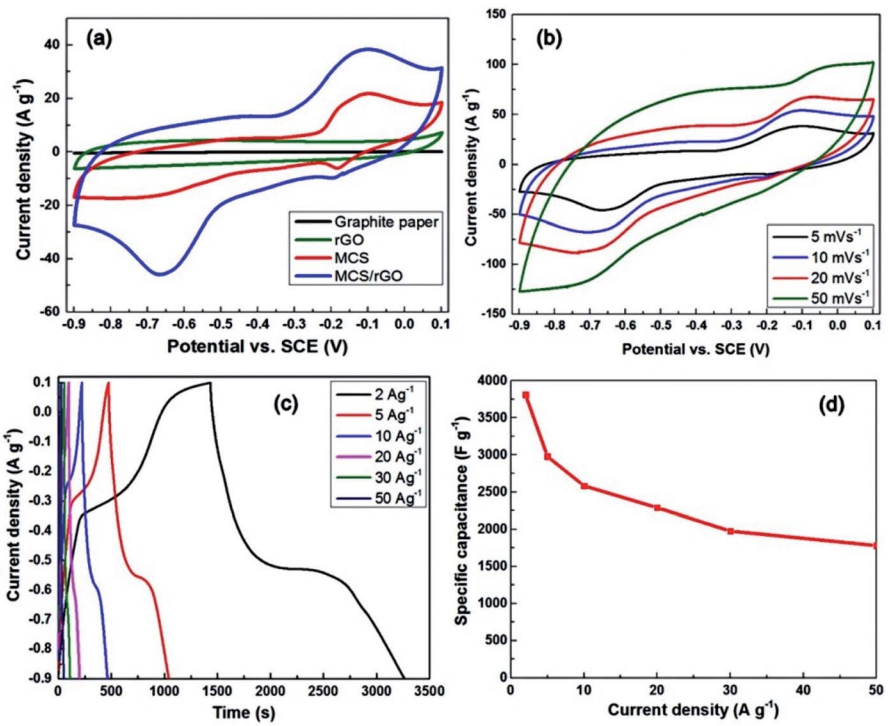

Fig. 4 (a) CV curves of the graphite paper substrate, MCS, rGO, and MCS/rGO at scan rate of 5 mV s^{-1}; (b) CV curves at different scan rates of MCS/rGO; (c) GCD curves of MCS/rGO at various current densities; (d) specific capacitance value of MCS/rGO as a function with the current density.

where the symbol I represents the discharge current (A), Δt is the discharge time (s), and m is the mass of the active material. The MCS/rGO electrode exhibits the highest C_{sp} value of 3812.5 F g^{-1} at a current density of 2 A g^{-1}, as shown in Fig. 4d. General, MCS nano-structure and MCS-based composites exhibit a high specific capacitance due to high oxidation potential of cobalt, high carrier concentration of manganese, and good conductivity of the composite (Table S1†). The capacitance decreases with increasing current density presenting values of 2976.8, 2582.7, 2288.9, 1976.4, and 1780.8 F g^{-1} at 5, 10, 20, 30, and 50 A g^{-1}, respectively. This behavior can be explained by the limited diffusion of electrolytic ions resulting in an inefficient charge storage capacity at high current densities. Nevertheless, it is important to note that the C_{sp} of the MCS/rGO electrode still reaches a fairly high value (1780.8 F g^{-1}) for a current density of 50 A g^{-1} indicating the excellent rate performance of electrode material. In addition, the discharge time of this material is larger than the charging time, which can be attributed to the irreversible reactions taking place during working process. The ligand exchange method with $NOBF_4$ and reduction of GO with ascorbic acid make the surface of the nanoparticles as well as the rGO foil to appear functional groups such as: –CO, –COOH, BF_4^-, *etc.* And K^+ ions in KOH electrolyte easily generate some irreversible chemical reactions.

Cycle endurance is a key parameter to evaluate the quality of SCs. As a result, cycling stability test for MCS/rGO electrode was carried out using constant current density of 50 A g^{-1} as shown in Fig. 5. MCS/rGO electrode displays great stability of 92.2% after 22 000 charge–discharge cycles. The enhancement in capacitance retention has been attributed to the electrochemical activation of the electrode surface, which is facilitated by the wettability of electrode material and electrolyte ions.[49] In addition, the hybrid MCS–rGO materials expanded the interlayer structure showing faster ion diffusion.[50,51] The gradual decrement in specific capacitance is mainly due to the conversion of metal sulfide to hydroxide under alkaline medium as well as the shedding and dissolution of the active material. In our recent study, the MCS-single nanosheet material only maintained 93% capacitance retention after 5000 duty cycles.[16]

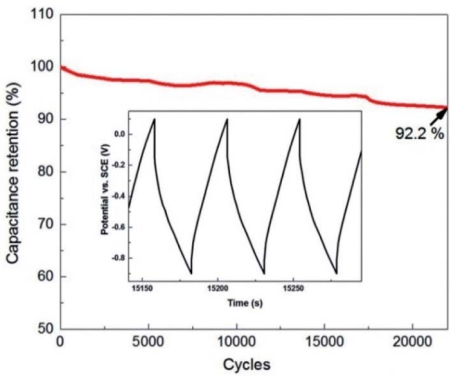

Fig. 5 Capacitance retention after 22 000 duty-cycles of the MCS/rGO electrode.

Therefore, the MCS material is degraded after undergoing a reversible redox reaction. Fig. S2† shows the CV curve of MCS/rGO before and after 22 000 duty cycles. It can be seen that the redox peak has been reduced, but the double layer capacitance is almost unchanged.

Electrochemical impedance spectrum analysis was also performed and an equivalent circuit model (ECM) for the MCS/rGO electrode was built accordingly. Fig. 6 shows the EIS Nyquist plot of the MCS/rGO electrode (including graphite paper substrate) and compares its EIS curve with equivalent circuit parameters before and after 22 000 duty cycles. The Nyquist curve is composed of a semicircle in the high-frequency region and a near linear in the low-frequency region. The smaller the radius of a semicircle, the lower the charge transfer resistance, and the larger the slope of the line results to better performance.[5,39] The inset in Fig. 6a shows an ECM, which has been matched to the measured EIS spectrum. The model includes: an equivalent series resistance (R_s); a resistance due to the redox reactions at the electrode/electrolyte interface (R_{ct}); a leak resistance (R_L); a double-layer capacitance (C_{DL}); a constant phase element (CPE_L) of non-ideal capacitor made from the junction between the active material and the graphite substrate; and a Warburg diffusion element (W) – representing the resistance of ionic diffusion in the electrolyte.[35] With this model, very low values of R_s (1.087 Ω) and R_{ct} (0.025 Ω) indicate good conductivities of MCS/rGO, along with easy ion exchange for reversible redox reactions. Thereby, the reversible redox reactions occur easily and repeat steadily during the charge/discharge process. In Fig. 6b, EIS of MCS/rGO electrode after 22 000 charge/discharge cycles shows that R_s and R_{ct} increased insignificantly (R_s is from 1.087 Ω to 1.172 Ω and R_{ct} is from 0.025 Ω to 0.078 Ω). This further confirms the contribution of rGO in the material system. rGO had high strength and low loss during the working life of the electrode.

The asymmetric supercapacitor with graphite powder as the negative electrode, MCS/rGO as the positive electrode and a cellulosic separator in 6 M KOH electrolyte was used to evaluate the electrochemical properties of the two-electrode system with working area of 2 × 1 cm^2. Fig. 7 shows the CV curve, GCD charge–discharge characteristic, EIS Nyquist plot, and the relationship between the power and energy of the full-cell supercapacitor. The CV curve is taken over the voltage range from 0 V to 1 V. The CV curve swells at the high potential range showing the redox properties of the MCS/rGO materials. From the GCD curves of the asymmetric device (Fig. 7b), the calculated capacitances are 316.2, 288.7, 244.7, 222.6, 200, and 157.7 F g^{-1} at the current densities of 1, 2, 5, 7.5, 10, and 15 A g^{-1}, respectively. The low specific capacitance and coulombic efficiency may be due to the reversible chemical reaction and ion exchange being limited by the separator and the two electrodes being tightly pressed together.[21,52] The EIS spectrum also shows that the internal resistance of the device increased (about 2.5 Ω, Fig. 7c). And, the maximum energy density of device achieves 43.91 W h kg^{-1} at a power density of 505 W kg^{-1}, and remains 21.9 W h kg^{-1} at 8762 W kg^{-1}.

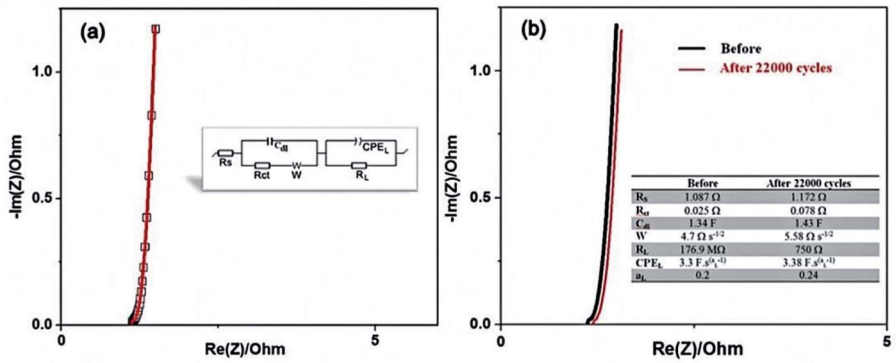

Fig. 6 EIS of (a) MCS/rGO electrode and its equivalent circuit model, (b) MCS/rGO electrode before and after 22 000 charging/discharging cycles.

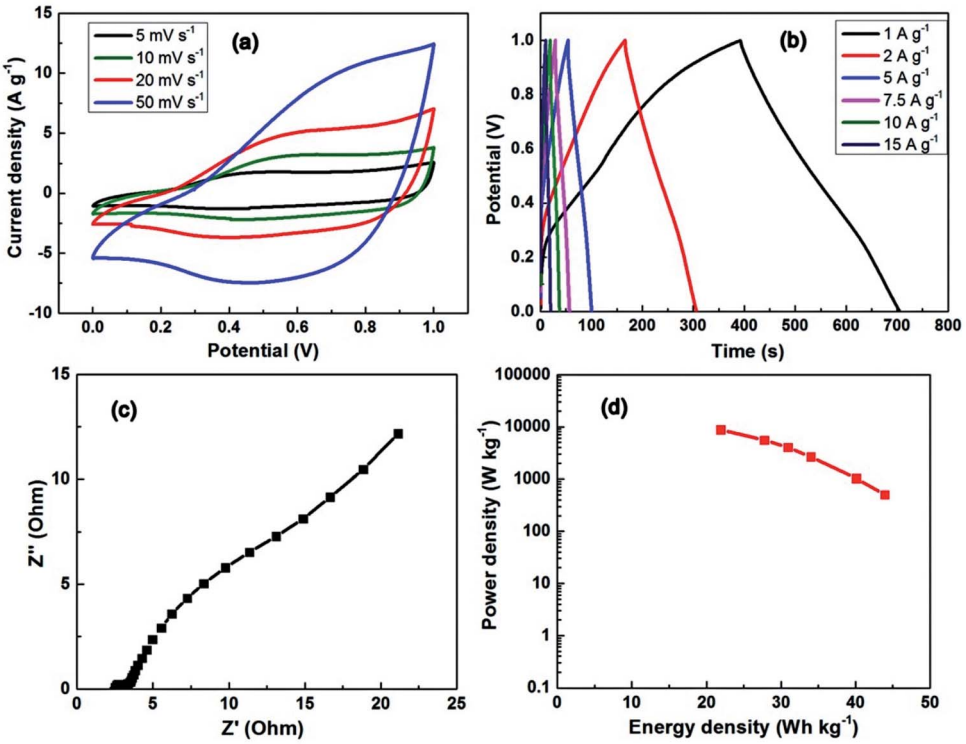

Fig. 7 (a) CV curves at various scanning rates, (b) GCD curves at various current densities, (c) EIS Nyquist plot, and (d) Ragone plot related to energy density and power density of the MCS–rGO symmetric full-cell supercapacitor.

4. Conclusions

In summary, MCS NPs, rGO, and MCS/rGO composites have been successful fabricated. The ink solution based on MCS/rGO composites was produced by simple and effective synthetic method, and it was used in 3D printing technique to prepare the electrodes. These techniques are promising large-scale and rapid production for practical applications. The as-prepared MCS/rGO electrode with anchoring of MCS NPs on the surface of the rGO sheets forms an interwoven structure facilitating access and diffusion of the electrolyte ions during charge/discharge process. The electrochemical behavior test results of MCS/rGO electrode show an ultrahigh specific capacitance of 3812.5 F g^{-1} at a current density of 2 A g^{-1} and a remaining high value of 1780.8 F g^{-1} at a current density of 50 A g^{-1}. The electrode also reveals the admirable cycling life time of 92.2% retention though 22 000 cycles at high current density (50 A g^{-1}). This work demonstrates that MCS/rGO composites are promising electrode materials for energy storage devices such as supercapacitors in the future.

Author contributions

H. M. N., L. T. T. T. and N. T. N. L. synthesized the MCS nanoparticles. L. T. T. T. and D. T. T. prepared the printing ink, and were major contributors in writing the manuscript. N. V. D. and H. T. D. modified the 3D printer, designed and printed the supercapacitor electrodes. N. T. D. and L. A. T. performed the analysis and assessment of the morphology and structure. L. T. T. T. and D. T. T. performed the measurements and analyzed the electrochemical results. L. T. L. and N. V. Q. designed experiments. D. V. and T. K. L. worked on the manuscript. L. T. L. and P. N. M. helped to supervise the project and improved the manuscript. All the authors read and approved the final manuscript.

Conflicts of interest

The authors declare that they have no competing interests.

Acknowledgements

This work was supported by the Vietnam National Foundation for Science and Technology Development (NAFOSTED) under Grant Number 103.02-2018.66.

References

1 J. Gao, X. Wang, X. Wang, R. Que, Y. Fang, B. Shi and Z. Wang, *RSC Adv.*, 2016, **6**, 68460–68467.
2 H. Li, L. Shen, J. Wang, S. Fang, Y. Zhang, H. Dou and X. Zhang, *J. Mater. Chem. A*, 2015, **3**, 16785–16790.
3 X. Han, H. Xuan, J. Gao, T. Liang, J. Yang, Y. Xu, P. Han and Y. Du, *Electrochim. Acta*, 2018, **288**, 31–41.
4 S. K. Sami, S. Siddiqui, M. T. Feroze and C. H. Chung, *Mater. Res. Express*, 2017, **4**, 116309.
5 F. Wang, K. Zhou, J. Zheng and J. Ma, *Synth. Met.*, 2019, **256**, 116113.
6 P. Sivasakthi, G. N. K. Ramesh Bapu, K. Murugavel and S. Mohan, *J. Alloys Compd.*, 2017, **709**, 240–247.
7 N. S. Arul, L. S. Cavalcante and J. In Han, *J. Solid State Electrochem.*, 2017, **22**, 303–313.
8 J. E. Zuliani, C. Q. Jia and D. W. Kirk, *J. Appl. Electrochem.*, 2017, **47**, 1213–1226.
9 H. Li, H. Xuan, Y. Guan, G. Zhang, R. Wang, X. Liang, Z. Xie, P. Han and Y. Wu, *Electrochim. Acta*, 2020, **345**, 136260.
10 Y. Liu, J. Zhang, S. Wang, K. Wang, Z. Chen and Q. Xu, *New J. Chem.*, 2014, **38**, 4045–4048.
11 J. Pu, F. Cui, S. Chu, T. Wang, E. Sheng and Z. Wang, *ACS Sustainable Chem. Eng.*, 2014, **2**, 809–815.
12 H. Zhou, S. Zhu, M. Hibino and I. Honma, *J. Power Sources*, 2003, **122**, 219–223.
13 K. J. Huang, J. Z. Zhang, G. W. Shi and Y. M. Liu, *Mater. Lett.*, 2014, **131**, 45–48.
14 X. Han, K. Tao, D. Wang and L. Han, *Nanoscale*, 2018, **10**, 2735–2741.
15 L. Liu, K. P. Annamalai and Y. Tao, *N. Carbon Mater.*, 2016, **31**, 336–342.
16 H. M. Nguyet, L. T. T. Tam, D. T. Tung, N. T. Yen, H. T. Dung, N. T. Dung, P. N. Hong, L. A. Tuan, P. N. Minh and L. T. Lu, Facile synthesis of $MnCo_2S_4$ nanosheets as a binder-free electrode material for high performance supercapacitor applications, *New J. Chem.*, 2022, DOI: **10.1039/D1NJ05809F**.
17 H. Wang, K. Zhang, Y. Song, J. Qiu, J. Wu and L. Yan, *Carbon*, 2019, **146**, 420–429.
18 Y. M. Chen, Z. Li and X. W. D. Lou, *Angew. Chem., Int. Ed.*, 2015, **54**, 10521–10524.
19 Y. Zhao, Z. Shi, H. Li and C. A. Wang, *J. Mater. Chem. A*, 2018, **6**, 12782–12793.
20 F. Zhang, M. Cho, T. Eom, C. Kang and H. Lee, *Ceram. Int.*, 2019, **45**, 20972–20976.
21 S. Sahoo and C. S. Rout, *Electrochim. Acta*, 2016, **220**, 57–66.
22 S. Liu and S. C. Jun, *J. Power Sources*, 2017, **342**, 629–637.
23 L. G. Beka, X. Li and W. Liu, *Sci. Rep.*, 2017, **7**, 2105.
24 H. Zhang, X. Zhang, D. Zhang, X. Sun, H. Lin, C. Wang and Y. Ma, *J. Phys. Chem. B*, 2013, **117**, 1616–1627.
25 X. Zhu, H. Dai, J. Hu, L. Ding and L. Jiang, *J. Power Sources*, 2012, **203**, 243–249.
26 T. Yao, X. Guo, S. Qin, F. Xia, Q. Li, Y. Li, Q. Chen, J. Li and D. He, *Nano-Micro Lett.*, 2017, **9**(4), 38.
27 X. Cai, X. Shen, L. Ma, Z. Ji and L. Kong, *RSC Adv.*, 2015, **5**, 58777–58783.
28 W. Peng, H. Chen, W. Wang, Y. Huang and G. Han, *Curr. Appl. Phys.*, 2020, **20**, 304–309.
29 Y. M. Fan, Y. Liu, X. Liu, Y. Liu and L. Z. Fan, *Electrochim. Acta*, 2017, **249**, 1–8.
30 Q. Li, N. Mahmood, J. Zhu, Y. Hou and S. Sun, *Nano Today*, 2014, **9**, 668–683.
31 K. Fu, Y. Wang, C. Yan, Y. Yao, Y. Chen, J. Dai, S. Lacey, Y. Wang, J. Wan, T. Li, Z. Wang, Y. Xu and L. Hu, *Adv. Mater.*, 2016, **28**, 2587.
32 L. T. T. Tam, D. T. Tung, N. T. Dung, P. N. Hong, P. V. Hoi, P. N. Minh and L. T. Lu, *Commun. Phys.*, 2020, **4**, 399–408.
33 L. T. T. Tam, N. V. Hung, D. T. Tung, N. T. Dung, H. T. Dung, P. T. Nam, P. N. Minh, P. N. Hong and L. T. Lu, *Vietnam J. Sci. Technol.*, 2019, **57**, 58.
34 D. T. Tung, L. T. T. Tam, H. T. Dung, N. T. Dung, N. Tuan-Dung, T. Hoang, T. D. Lam, P. N. Minh, T. V. Thu, P. N. Hong and L. T. Lu, *J. Electron. Mater.*, 2020, **49**, 4671.
35 D. T. Tung, L. T. T. Tam, H. T. Dung, N. T. Dung, P. N. Hong, H. M. Nguyet, N. Van-Quynh, N. V. Chuc, V. Q. Trung, L. T. Lu and P. N. Minh, *Electrochim. Acta*, 2021, **392**, 138992.
36 Z. Tang, Z. Zhang, Z. Han, S. Shen, J. Li and J. Yang, *J. Mater. Sci.*, 2016, **51**, 8791–8798.
37 W. Wei and X. Qu, *Small*, 2012, **8**, 2138–2151.
38 C. Wu, Q. Cheng, K. B. Wu, G. Wu and Q. Li, *Anal. Chim. Acta*, 2014, **825**, 26.
39 T. K. Enock, C. K. King'ondu, A. Pogrebnoi and Y. A. C. Jande, *Mater. Today Energy*, 2017, **5**, 126–137.
40 X. Xia, C. Zhu, J. Luo, Z. Zeng, C. Guan, C. F. Ng, H. Zhang and H. J. Fan, *Small*, 2014, **10**, 766–773.
41 T. Chen, Y. Tang, Y. Qiao, Z. Liu, W. Guo, J. Song, S. Mu, S. Yu, Y. Zhao and F. Gao, *Sci. Rep.*, 2016, **6**, 23289.
42 Y. Tang, T. Chen and S. Yu, *Chem. Commun.*, 2015, **51**, 9018–9021.

43 Q. Zhang, C. Xu and B. Lu, *Electrochim. Acta*, 2014, **132**, 180–185.
44 J. Shi, X. Li, G. He, L. Zhang and M. Li, *J. Mater. Chem. A*, 2015, **3**, 20619–20626.
45 Y. Zhu, Z. Wu, M. Jing, X. Yang, W. Song and X. Ji, *J. Power Sources*, 2015, **273**, 584–590.
46 X. Li, J. Shen, N. Li and M. Ye, *J. Power Sources*, 2015, **282**, 194–201.
47 R. Chen, L. Liu, J. Zhou, L. Hou and F. Gao, *J. Power Sources*, 2017, **341**, 75–82.
48 Y. Zhu, X. Ji, H. Chen, L. Xi, W. Gong and Y. Liu, *RSC Adv.*, 2016, **6**, 84236–84241.
49 W. Liu, H. Niu, J. Yang, K. Cheng, K. Ye, K. Zhu, G. Wang, D. Cao and J. Yan, *Chem. Mater.*, 2018, **30**, 1055–1068.
50 Q. Liu, X. Hong, X. You, X. Zhang, X. Zhao, M. Ye and X. Liu, *Energy Storage Mater.*, 2020, **24**, 541–549.
51 C. Zhan, W. Liu, M. Hu, Q. Liang, X. Yu, Y. Shen, R. Lv and F. Kang, *NPG Asia Mater.*, 2018, **10**, 775–787.
52 X. Hu, S. Liu, Y. Chen, J. Jiang, H. Cong, J. Tang, Y. Sun, S. Han and H. Lin, *New J. Chem.*, 2020, **44**, 11786.